

**Competition between crystallization and gelation: A local description**

Narendra M. Dixit\* and Charles F. Zukoski†

*Department of Chemical and Biomolecular Engineering, University of Illinois at Urbana-Champaign, 114, Roger Adams Laboratory, 600 South Mathews Avenue, Urbana, Illinois 61801*

(Received 15 November 2002; published 2 June 2003)

We develop a model to describe the competition between gelation and crystallization in colloidal suspensions where particle interactions are represented by square well attractions. The competition is discussed locally in terms of the tendencies of individual particles to attain amorphous or crystalline configurations on cluster surfaces. These tendencies are dictated by three independent processes, the aggregation of particles onto, the dissociation of particles from, and the rearrangement of particles on the cluster surfaces. Models are developed to determine the rates of each of these processes. The relative magnitudes of these rates determine the probability that a particle arriving onto a cluster surface reaches a crystalline configuration, remains arrested in an amorphous configuration, or dissociates back into the suspension. These probabilities are employed to determine whether stable crystalline or amorphous clusters nucleate, resulting in predictions of the occurrence of crystallization or gelation as a function of solution conditions. Comparisons of model predictions with recent experiments on globular protein suspensions show excellent agreement, suggesting that the model captures much of the underlying physics of the competition between gelation and crystallization in attractive colloidal suspensions.

DOI: 10.1103/PhysRevE.67.061501

PACS number(s): 82.70.-y, 81.10.-h

**I. INTRODUCTION**

Upon quenching a suspension of particles experiencing attractive interactions, crystallization can be preempted by a nonequilibrium gel transition [1,2]. The gel phase thus formed has unique properties: it is solidlike in that it does not flow and can bear a nonzero shear stress, and is liquidlike in that it lacks a structure with long range order. Gels often have self-similar structures that span space to form a percolated network at packing fractions significantly lower than packing fractions in ordinary solids [3]. Accordingly, colloidal gels are employed extensively in the paints, coatings, foods, drug, and cosmetics industries. On the other hand, the gel phase can be a hindrance to crystal formation. Highly ordered crystalline solids are indispensable in the identification of protein structures, the manufacture of photonic band gap materials, and controlled drug delivery [4–7]. In such applications, the gel phase is undesirable. For systems that crystallize, little is known about how to control the competition between gelation and crystallization [8–12]. Understanding how to control this competition is clearly an area that has widespread consequences.

Equilibrium thermodynamics predicts the occurrence of crystals as the stable thermodynamic phase upon crossing the solubility boundary [13]. The location of the solubility boundary in a temperature-concentration phase diagram depends on the details of the interactions between the particles. Gelation, on the other hand, is a purely kinetic transition and is not predicted by thermodynamic approaches. Alternative approaches have been developed wherein signatures of the gel phase are employed as the criteria to predict the occur-

rence of gelation. For example, the percolation threshold, which indicates the formation of a cluster large enough to span the expanse of the system, has been used to delineate conditions where gels may occur [14,15]. In the more recent mode coupling approach, recognizing that gels are nonergodic states, conditions yielding nontrivial solutions for the nonergodicity parameters are used to suggest the formation of gels [16]. While useful in predicting the location of nonergodic transitions, these approaches cannot address the competition between gelation and crystallization. As a result, whether a gel or crystals will result under given solution conditions remains poorly understood.

Experimental studies on hard-sphere colloidal suspensions where a depletion attraction is induced between the particles by adding nonadsorbing polymer demonstrate the prevalent competition between gelation and crystallization [8–11]. For short ranges of attraction (set by a small polymer-to-colloid size ratio), gelation preempts crystallization upon increasing either the colloid or the polymer concentration. At a fixed polymer concentration, which determines the strength of the depletion attraction, increasing the polymer-to-colloid size ratio results in crystallization. In more recent studies on globular protein suspensions [12], crystals were observed to nucleate directly from the fluid phase at higher strengths of attraction, whereas at lower strengths of attraction, the suspensions gelled at short times with crystals nucleating from the gels at very long times. These studies point to the subtle and poorly understood effects of changing the strength and the range of particle attractions on the resulting gelation and crystallization transitions.

While gels and crystals have drastically different properties, the processes that lead to their formation are identical at the molecular level: Both gels and crystals are formed as consequences of particle aggregation and dissociation processes. Particles aggregate via Brownian encounters. Depending on the strength of the attractions between the par-

\*Present address: Theoretical Division, Los Alamos National Laboratory, MS K710, Los Alamos, NM 87545.

†Author to whom all correspondence should be addressed. Email address: czukoski@uiuc.edu

ticles relative to their thermal energy, the particles rearrange into ordered structures over varying time scales. Thermal fluctuations allow bound particles to dissociate into the suspension. The relative rates of these processes determine whether gels or crystals will eventually result: When rearrangement is rapid, and therefore complete, equilibrium structures, or crystals, result. When rearrangement is incomplete, particles remain arrested in nonequilibrium configurations yielding amorphous aggregates and gels. Extant models fail to recognize this similarity in the underlying processes; while gelation is treated as a dynamic nonergodicity transition [16], crystallization is understood using the completely independent framework of equilibrium thermodynamics [13]. As a result, difficulties arise in addressing the competition between gelation and crystallization. Here, recognizing the similarity in the underlying processes, we develop a model that employs descriptions of these processes and predicts the occurrence of gelation and crystallization as a function of solution conditions.

Particle aggregation and dissociation are central to the theories of crystal nucleation. In previous studies, a description of these processes in the context of crystallization in hard sphere [17,18] and attractive colloidal suspensions [19,20] has been developed. Here, we consider square well systems as the equilibrium thermodynamics of these systems is well understood and independent predictions of percolation [22], gelation [11], and crystallization [23] in these systems have been reported. Further, square wells form an excellent model to elucidate the effects of systematically changing the strength and the range of attractions on the resulting phase behavior. To describe particle rearrangement, we assume that upon aggregation individual particles diffuse independently to locations where their energies are minimized. Cooperative rearrangement is neglected, and the rearrangement time of individual particles is determined using a mean first passage time analysis. From the rates of particle aggregation, dissociation, and rearrangement, we are able to calculate the probability that a particle diffuses to its local free energy minimum or remains trapped in amorphous locations. Falling into the local free energy minimum is considered to result in crystallization while being trapped is considered to result in gelation. We compare our predictions with recent experiments on globular protein suspensions and find excellent agreement. We conclude that the present description captures much of the underlying physics that dictates the competition between gelation and crystallization in attractive colloidal suspensions.

The paper is organized as follows. We begin in Sec. II with a brief description of the equilibrium thermodynamics of square well systems. In Sec. III, we present our model for calculating the probabilities of crystalline versus amorphous cluster formation as functions of the time scales of particle aggregation, dissociation, and rearrangement processes. Calculations of these time scales are described in Sec. IV. In Sec. V, we present model predictions of the occurrence of gelation and crystallization as a function of solution conditions and compare them with experiments on globular proteins. We draw conclusions in Sec. VI.

## II. EQUILIBRIUM THERMODYNAMICS OF SQUARE WELL SYSTEMS

Consider a suspension of spherical particles of radii “ $a$ ” interacting with a dimensionless pair potential given by the centrosymmetric square well

$$\frac{U(r)}{kT} = \begin{cases} \infty, & r \leq 2a \\ -\varepsilon/kT, & 2a < r \leq 2\lambda a \\ 0, & r > 2\lambda a, \end{cases} \quad (1)$$

where  $r$  is the center-to-center separation of a pair of particles,  $\varepsilon$  is the strength of the attraction between the particles,  $\lambda$  is the range of the attraction, and  $kT$  is the product of Boltzmann constant and the absolute temperature. Many studies have been carried out detailing the equilibrium thermodynamics of such a suspension [23–26]. An equation of state for the fluid phase has been proposed [23]:

$$\frac{Pa^3}{\phi kT} = \frac{3}{4\pi} \left[ 1 + \frac{b\phi}{\left(1 - \frac{\phi}{\phi_o}\right)^2} + \frac{6}{\pi} \frac{(\varepsilon/kT)\phi f(\lambda)}{\left(1 - \frac{\phi}{\phi_b}\right)^3} \right], \quad (2)$$

where  $P$  is the osmotic pressure,  $\phi$  is the particle volume fraction,  $b=4$  and  $\phi_o=0.84$  are constants, and  $\phi_b$  and  $f(\lambda)$  are both tabulated functions of  $\lambda$  [23]. From this, the chemical potential of a particle in the fluid phase is calculated as [19]

$$\mu_l = \int_0^\phi \left( \frac{4\pi}{3} \frac{Pa^3}{\phi' kT} - 1 \right) \frac{d\phi'}{\phi'} + \frac{4\pi}{3} \frac{Pa^3}{\phi kT} + \ln(\phi) - 1. \quad (3)$$

The fluid-fluid phase separation boundary, or the binodal, is determined using the conditions  $P^I = P^{II}$  and  $\mu_l^I = \mu_l^{II}$ , where I and II correspond to the dilute and dense fluid phases in equilibrium. The locus of points that satisfy  $dP/d\phi = 0$  gives the spinodal. The spinodal and the binodal meet at the critical point. The fluid-crystal phase boundary or the solubility boundary, is determined by the condition  $\mu_l = \mu_s$ , where  $\mu_s$  is the chemical potential of a particle in the crystalline phase, calculated as [19]

$$\mu_s = -C\varepsilon/2kT - 3 \ln(\lambda - 1), \quad (4)$$

where  $C=12$  is the number of nearest neighbors of particles in the crystalline phase, and the solid is assumed to be incompressible. For  $\lambda < 1.35$ , the fluid-fluid phase separation is metastable with respect to the fluid-crystal phase separation, whereas stable fluid-fluid phase separation conditions are predicted for  $\lambda > 1.35$  [19].

Comparison of model predictions with experiments requires linking the parameters  $\varepsilon$  and  $\lambda$  to experimental measures of particle interactions. One method employed, especially in studies of globular protein suspensions, is to link parameters in the interaction energy to the measurable property  $B_2$ , the second virial coefficient of the osmotic pressure

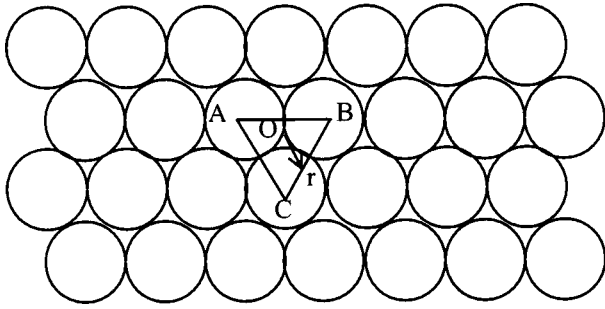


FIG. 1. Triangular lattice assumed to describe rearrangement of particles on cluster surfaces. Triangle ABC marks a representative lattice unit. The centroid O of the triangle is chosen as the origin of the polar coordinate system to describe particle motion.

of the colloidal suspension [27].  $B_2$  is an integral measure of particle interactions and is given for square well systems by

$$\frac{B_2}{B_2^{HS}} = 1 - (e^{\varepsilon/kT} - 1)(\lambda^3 - 1), \quad (5)$$

where  $B_2^{HS} = 16\pi a^3/3$  is the second virial coefficient for particles interacting with a hard-sphere potential. Generalized phase diagrams have been developed for  $0 < (\lambda - 1) \ll 1$ , where  $B_2$  is shown to be correlated with the equilibrium solubility of a wide variety of globular protein and colloidal suspensions [27,28]. The above description captures the correlation quite accurately indicating the ability of the square well model to describe protein solution thermodynamics [23]. However, the model fails to capture the location of the metastable spinodal [12,29]. Here, we employ this description of square well systems to understand the competition between gelation and crystallization.

### III. LOCAL DESCRIPTION OF CLUSTER FORMATION: CRYSTALLINE VERSUS AMORPHOUS AGGREGATES

In a supersaturated suspension, where  $\phi > \phi_s$ , the equilibrium solubility at any given  $\varepsilon/kT$ , particles aggregate to form growing clusters. When the attractions are short ranged, Brownian encounters between particles in a dilute suspension result in clusters with open, fractal-like particle configurations; at best, the particles are randomly close packed. Subsequently, however, these particles tend to rearrange into crystalline configurations in order to minimize their free energies. At the same time, particles on cluster surfaces constantly undergo thermal motion, which allows them to dissociate back into the suspension. Thus, three processes, particle aggregation, dissociation, and rearrangement, continually occur, and determine cluster growth. We argue that the formation of crystalline configurations results in macroscopic crystals, whereas the formation of amorphous clusters, when space filling, eventually causes the suspension to gel.

To determine order within a cluster, we consider the aggregation of particles onto a perfectly crystalline cluster surface. Assuming the cluster to be large, we represent it by a two-dimensional lattice as shown in Fig. 1. Without loss of

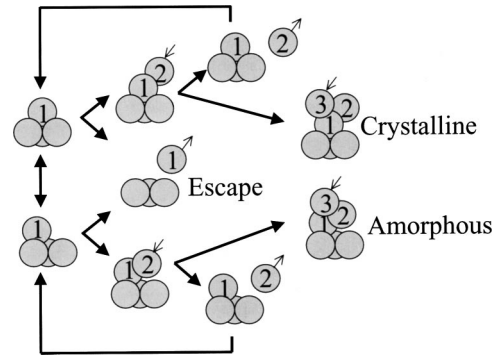


FIG. 2. A schematic of the possible events that a particle, particle 1, on a cluster surface may experience. The bold arrows represent the sequence of possible events. The thin arrows indicate actual motion of particles. The un-numbered particles represent a lattice unit on the cluster surface.

generality, we let the lattice to be triangular. Let a particle, say particle 1, arrive onto the cluster surface at a time  $t = 0$ . We assume that the particle arrives at an arbitrary position on the surface, onto a representative lattice unit ABC. A zone around the centroid of triangle ABC represents the nearest free energy minimum location for the particle. The larger the range of particle attractions, the bigger is this zone. Energetically equivalent but distant locations exist around the centroids of other similar lattice units. Consider now a suspension above the perfect cluster surface. Brownian encounters will result in cluster growth if the suspension is supersaturated. A particle, particle 1, arriving at the surface will undergo surface diffusion and have a biased path towards the zone that minimizes its energy. Or, it may arrive inside the zone and diffuse out due to thermal motion. During this diffusion, it may get trapped in an amorphous (outside the zone) or a crystalline (inside the zone) configuration due to the arrival of additional particles, or may leave the cluster and dissociate back into the suspension via thermal motion. A crystalline (amorphous) cluster grows every time such a particle is arrested in a crystalline (amorphous) location. Our aim is to determine whether a particle arriving on the cluster surface ends its excursion on the surface in a crystalline or an amorphous configuration. The result is a local description of crystalline and amorphous cluster formation.

We consider first the case when particle 1 arrives onto the cluster surface at an amorphous location in the arbitrary unit ABC. To minimize its free energy, the particle diffuses towards the crystalline zone in the center of ABC. This rearrangement process of particle 1 has two constraints. First, it requires that particle 1 does not dissociate back into the suspension before the rearrangement is complete. The second constraint is introduced by the arrival of another particle, say particle 2, onto the cluster surface at a location that allows bond formation between particles 1 and 2. When this happens, the rearrangement of particle 1 is no longer independent. Particle 1 must either break its bond with particle 2 or the two must rearrange cooperatively. While cooperative rearrangement is possible, we assume that it occurs extremely slowly so that particle 1 is essentially arrested in its position

unless it breaks its bond with particle 2. We assume further that the bond between particles 1 and 2 is broken by the dissociation of the latter back into the suspension via thermal motion. This process can continue recursively with particles 3, 4, 5, . . . aggregating onto particles 1 and 2. For simplicity, we assume that if particle 3 arrives onto particles 1 and 2, it becomes extremely difficult for particle 2 to diffuse back into the suspension, resulting in the arrest of the rearrangement process of particle 1. Particle 1 then remains caught in an amorphous configuration. This description is shown schematically in Fig. 2. Below, we determine the probability that particle 1, having arrived at an amorphous location, is able to reach a crystalline configuration and the probability that it is arrested in an amorphous location in terms of the time scales of the aggregation, dissociation, and rearrangement processes.

Let the average dissociation time of particles from amorphous locations be  $t_\alpha$ . Then, assuming that the dissociation of every particle is an independent process, the probability that the dissociation time of particle 1 is within  $dt$  of  $t$  equals  $f_\alpha(t)dt$ , where

$$f_\alpha(t) = (1/t_\alpha)\exp(-t/t_\alpha) \quad (6)$$

is the probability density of the dissociation process. Similarly,

$$f_\beta(t) = (1/t_\beta)\exp(-t/t_\beta) \quad (7)$$

and

$$f_\gamma(t) = (1/t_\gamma)\exp(-t/t_\gamma), \quad (8)$$

define the probability densities of the aggregation and rearrangement processes, respectively, where  $t_\beta$  is the average aggregation time of particles to within a bond forming distance of an existing particle on a cluster surface and  $t_\gamma$  the average time for the rearrangement of aggregated particles from amorphous to crystalline locations. We assume that the three processes occur independently of each other. Let  $t_{d-1}$  denote the time after arriving onto a cluster surface when particle 1 dissociates back into the suspension and  $t_{r-1}$  the time when particle 1 reaches a crystalline location. Let  $t_{a-2}$  denote the time when particle 2 aggregates onto the cluster surface to within a bond forming distance of particle 1. Then, particle 1 is able to reach a crystalline location if  $t_{r-1}$  is smaller than  $t_{d-1}$  and  $t_{a-2}$ . A second way for particle 1 to reach a crystalline location is if  $t_{a-2}$  is smaller than  $t_{d-1}$  and  $t_{r-1}$ , but particle 2 dissociates before particle 3 arrives, i.e.,  $t_{d-2}$  is less than  $t_{a-3}$ . Once particle 2 dissociates, we reset the clock, so that particle 1 can reach a crystalline site again if  $t_{r-1}$  is smaller than  $t_{d-1}$  and  $t_{a-2}$ . Again, this description is shown schematically in Fig. 2. Thus, if  $P_r$  is the probability that particle 1 reaches the crystalline location, we have

$$\begin{aligned} P_r &= P(t_{r-1} < (t_{d-1} \text{ and } t_{a-2})) \\ &+ P(t_{a-2} < (t_{d-1} \text{ and } t_{r-1}))P(t_{d-2} < t_{a-3})P_r \\ &= \int_{t_r=0}^{\infty} \int_{t_a=t_r}^{\infty} \int_{t_d=t_r}^{\infty} f_\alpha(t_d)f_\beta(t_a)f_\gamma(t_r)dt_d dt_a dt_r \\ &+ \left[ \int_{t_a=0}^{\infty} \int_{t_r=t_a}^{\infty} \int_{t_d=t_a}^{\infty} f_\alpha(t_d)f_\beta(t_a)f_\gamma(t_r)dt_d dt_a dt_r \right] \\ &\times \left[ \int_{t_d=0}^{\infty} \int_{t_a=t_d}^{\infty} f_\alpha(t_d)f_\beta(t_a)dt_a dt_d \right] P_r, \quad (9) \end{aligned}$$

where in the latter equality, the second subscript on the times, which identifies the particle number, has been dropped because all particles are assumed to follow the same statistics, given by Eqs. (6)–(8) above, for the aggregation, dissociation, and rearrangement times. Upon simplification, Eq. (9) yields

$$P_r = \frac{\frac{1}{t_\gamma}}{\frac{1}{t_\alpha} + \frac{1}{t_\beta} + \frac{1}{t_\gamma}} \cdot \frac{1}{1 - \left[ \frac{\frac{1}{t_\beta}}{\frac{1}{t_\alpha} + \frac{1}{t_\beta} + \frac{1}{t_\gamma}} \right] \left[ \frac{\frac{1}{t_\alpha}}{\frac{1}{t_\alpha} + \frac{1}{t_\beta}} \right]}. \quad (10)$$

Similarly, the probability  $P_a$  that particle 1 remains arrested in an amorphous location is given by (Fig. 2):  $P_a = P(t_{a-2} < (t_{d-1} \text{ and } t_{r-1})) [P(t_{a-3} < t_{d-2}) + P(t_{d-2} < t_{a-3})P_a]$ , so that

$$P_a = \frac{\left[ \frac{\frac{1}{t_\beta}}{\frac{1}{t_\alpha} + \frac{1}{t_\beta} + \frac{1}{t_\gamma}} \right] \left[ \frac{\frac{1}{t_\beta}}{\frac{1}{t_\alpha} + \frac{1}{t_\beta}} \right]}{1 - \left[ \frac{\frac{1}{t_\beta}}{\frac{1}{t_\alpha} + \frac{1}{t_\beta} + \frac{1}{t_\gamma}} \right] \left[ \frac{\frac{1}{t_\alpha}}{\frac{1}{t_\alpha} + \frac{1}{t_\beta}} \right]}. \quad (11)$$

If particle 1 neither reaches a crystalline location nor gets arrested in an amorphous location, it leaves the surface from an amorphous location and escapes into the suspension. The probability that this happens is given by  $P_l = P(t_{d-2} < (t_{a-2} \text{ and } t_{r-1})) + P(t_{a-2} < (t_{d-1} \text{ and } t_{r-1}))P(t_{d-2} < t_{a-3})P_l$ , or

$$P_l = \frac{\frac{1}{t_\alpha}}{\frac{1}{t_\alpha} + \frac{1}{t_\beta} + \frac{1}{t_\gamma}} \cdot \left[ \frac{\frac{1}{t_\beta}}{\frac{1}{t_\alpha} + \frac{1}{t_\beta} + \frac{1}{t_\gamma}} \right] \cdot \left[ \frac{\frac{1}{t_\alpha}}{\frac{1}{t_\alpha} + \frac{1}{t_\beta}} \right]. \quad (12)$$

It is easily verified that  $P_r + P_a + P_l = 1$ .

Next, we consider the case where particle 1 arrives on the surface in a crystalline configuration, i.e., its diffusive trajectory in the suspension causes it to arrive near the centroid of Fig. 1. As depicted in Fig. 2, particle 1 may then dissociate back into the suspension, diffuse on the cluster surface to an amorphous location, or remain arrested in the crystalline configuration. If the probabilities for these events are  $P_{lx}$ ,  $P_{rx}$ , and  $P_{ax}$ , respectively, then following the above description, we can write

$$P_{rx} = \frac{\frac{1}{t_{\gamma x}}}{\frac{1}{t_{\alpha x}} + \frac{1}{t_\beta} + \frac{1}{t_{\gamma x}}} \cdot \left[ \frac{\frac{1}{t_\beta}}{\frac{1}{t_{\alpha x}} + \frac{1}{t_\beta} + \frac{1}{t_{\gamma x}}} \right] \cdot \left[ \frac{\frac{1}{t_{\alpha x}}}{\frac{1}{t_{\alpha x}} + \frac{1}{t_\beta}} \right], \quad (13)$$

$$P_{ax} = \frac{\left[ \frac{\frac{1}{t_\beta}}{\frac{1}{t_{\alpha x}} + \frac{1}{t_\beta} + \frac{1}{t_{\gamma x}}} \right] \cdot \left[ \frac{\frac{1}{t_\beta}}{\frac{1}{t_{\alpha x}} + \frac{1}{t_\beta}} \right]}{1 - \left[ \frac{\frac{1}{t_\beta}}{\frac{1}{t_{\alpha x}} + \frac{1}{t_\beta} + \frac{1}{t_{\gamma x}}} \right] \cdot \left[ \frac{\frac{1}{t_{\alpha x}}}{\frac{1}{t_{\alpha x}} + \frac{1}{t_\beta}} \right]}, \quad (14)$$

and

$$P_{lx} = \frac{\frac{1}{t_{\alpha x}}}{\frac{1}{t_{\alpha x}} + \frac{1}{t_\beta} + \frac{1}{t_{\gamma x}}} \cdot \left[ \frac{\frac{1}{t_\beta}}{\frac{1}{t_{\alpha x}} + \frac{1}{t_\beta} + \frac{1}{t_{\gamma x}}} \right] \cdot \left[ \frac{\frac{1}{t_{\alpha x}}}{\frac{1}{t_{\alpha x}} + \frac{1}{t_\beta}} \right], \quad (15)$$

where  $t_{\alpha x}$  and  $t_{\gamma x}$  are the time scales for the dissociation and the rearrangement, respectively, of a particle in a crystalline location. Here, by rearrangement is meant the diffusion of

the particle to an amorphous location. Since a particle arriving from the bulk suspension does not distinguish between a particle in a crystalline or an amorphous location, the aggregation time onto both remains the same, viz.,  $t_\beta$ . Here, the range of attraction is assumed to be sufficiently small so that any steering of arriving particles into lower energy crystalline configurations can be neglected.

Our aim is to determine the likelihood of a particle arriving onto a cluster surface ending its excursion on the surface in a crystalline or an amorphous location. Let  $f$  be the probability that a particle arrives onto the surface at a crystalline site. Let  $P_{c1}$  be the probability that such a particle ends its excursion in a crystalline location. Let  $P_{c2}$  be the probability that a particle arriving at an amorphous location ends its excursion in a crystalline location. Then, the probability that a particle arriving at an arbitrary location—crystalline or amorphous—ends its excursion in a crystalline location is given by  $P_{\text{crystal}} = fP_{c1} + (1-f)P_{c2}$ . The probabilities  $P_{c1}$  and  $P_{c2}$  are linked through the equations:  $P_{c1} = P_{ax} + P_{rx}P_{c2}$  and  $P_{c2} = P_rP_{c1}$ . The first equation indicates that a particle arriving onto a crystalline location is eventually arrested in a crystalline location if it gets arrested there upon arrival (first term) or if it diffuses to an amorphous location and is subsequently arrested in a crystalline location (second term). The latter probability is determined by the second equation as the product of the probabilities of a particle in an amorphous location reaching a crystalline location and subsequently getting arrested there. Solving these simultaneous equations, it follows that

$$P_{\text{crystal}} = [f + (1-f)P_r] \left( \frac{P_{ax}}{1 - P_rP_{rx}} \right). \quad (16)$$

Similarly, the probability  $P_{\text{gel}}$  that a particle arriving at an arbitrary location on the surface ends its excursions at an amorphous location is given by

$$P_{\text{gel}} = [fP_{rx} + (1-f)] \left( \frac{P_a}{1 - P_rP_{rx}} \right). \quad (17)$$

Thus, the probability that a particle arriving onto a crystalline surface is eventually arrested in a crystalline or an amorphous configuration can be calculated given the time scales of the aggregation, dissociation, and rearrangement processes, viz.,  $t_\alpha$ ,  $t_\beta$ ,  $t_\gamma$ ,  $t_{\alpha x}$ , and  $t_{\gamma x}$ , and the parameters  $f$ ,  $C_{x\infty}$ , and  $\zeta$ . Below, we present models to calculate these quantities as functions of solution conditions, viz.  $\phi$ ,  $\varepsilon/kT$ , and  $\lambda$ .

#### IV. PARTICLE DISSOCIATION, AGGREGATION, AND REARRANGEMENT PROCESSES

##### A. Dissociation

Descriptions of the aggregation and dissociation processes for square well systems have been developed previously [19]. A spherical cluster of radius  $R$  is considered. To determine dissociation rates, particles on the cluster surface are assumed to reside in potential energy wells because of their bonds with nearest neighbors. The motion of the particles in

these potential wells is described by the Smoluchowski equation. Solving the Smoluchowski equation, the average time required for the particles to diffuse out of their potential wells into the bulk suspension is determined. This dissociation time depends on the depth of the potential well holding the particles,  $\Phi = -C_s \varepsilon / kT$ , where  $C_s$  is the number of nearest neighbors of a particle on the cluster surface (the number of nearest neighbors of a particle in a fluid is assumed negligible).  $C_s$  depends on  $R$  as well as on whether the particle is in an amorphous or a crystalline location. For a particle in a crystalline location, the following empirical form has been suggested [17,18]

$$C_{sx}(R) = 1 + (C_{x\infty} - 1)[1 - \exp\{\zeta(R_{\min} - R)/2a\}], \quad (18)$$

where  $C_{x\infty}$  is the number of nearest neighbors of a particle in a crystalline configuration on the surface of an infinitely large crystalline cluster.  $R_{\min} = a(2/0.74)^{1/3}$  is the radius of the smallest possible cluster, i.e., containing two particles. A particle in such a cluster has one nearest neighbor. The parameter  $\zeta$  characterizes how  $C_{sx}$  varies as  $R$  increases beyond  $R_{\min}$  and is related to the curvature dependence of the solid-fluid surface tension [17,18]. Determination of the parameters  $\zeta$  and  $C_{x\infty}$  is discussed below.

To determine the number of nearest neighbors of a particle in an amorphous location  $C_s$ , we note that when  $R = R_{\min}$ ,  $C_s = C_{sx} = 1$ , whereas on an infinitely large crystalline cluster surface,  $C_{x\infty} - C_{s\infty}$  is either 1 or 2 for a triangular lattice. Here, we let this difference be 1.5, and assuming that  $C_s$  increases with  $R$  in a manner similar to  $C_{sx}$ , we write

$$C_s(R) = 1 + (C_{x\infty} - 1.5 - 1)[1 - \exp\{\zeta(R_{\min} - R)/2a\}]. \quad (19)$$

With these assumptions, the Smoluchowski equation gives the dissociation times as [17–19]

$$t_\alpha = \frac{R^2 \exp\{C_s \varepsilon / kT\} (1 + d/R)^3 - 1}{3D_o \omega} \frac{1}{(1 + d/R)^2} \quad (20)$$

and

$$t_{\alpha x} = \frac{R^2 \exp\{C_{sx} \varepsilon / kT\} (1 + d/R)^3 - 1}{3D_o \omega} \frac{1}{(1 + d/R)^2}, \quad (21)$$

where  $d = 2a(\lambda - 1)$  is the width of the well holding the particles;  $D_o$  is the Stokes-Einstein diffusivity of the particles; and  $\omega = 0.2$  is an approximate hydrodynamic correction to  $D_o$  on the cluster surface [19]. The size dependencies of the number of nearest neighbors ensure that particles dissociate from small clusters faster than they dissociate from large clusters.

### B. Aggregation

As particles compact into clusters, a small zone around the clusters becomes depleted of monomers. This generates a gradient in the concentration of monomers from the bulk suspension to the cluster surfaces. Particles are assumed to aggregate onto cluster surfaces by diffusing down this con-

centration gradient. Assuming that the concentration of particles in the depletion zone is negligible, the diffusion equation is solved to give the steady state rate of particles aggregating onto the cluster surface [19]:

$$\beta = \frac{3R}{a^3} \left(1 + \frac{d}{R}\right) \int_0^\phi D(\phi') d\phi', \quad (22)$$

where  $\phi$  is the volume fraction of particles in the bulk suspension and  $D(\phi)$  is the gradient diffusivity of the particles, given by [13,19]

$$D(\phi) = D_o K(\phi) \frac{d}{d\phi} [\phi Z(\phi)], \quad (23)$$

where  $Z(\phi) = 4\pi P a^3 / 3\phi kT$  is calculated via Eq. (2), and  $K(\phi) = (1 - \phi)^{-K_2}$ , with

$$K_2 = -6.567 + 4.056 \left(1 - \frac{B_2}{B_2^{HS}}\right), \quad (24)$$

where  $B_2/B_2^{HS}$  is given by Eq. (5) [13,19].

Equations (22)–(24) thus allow the calculation of  $\beta$ , the rate at which particles aggregate onto a cluster of radius  $R$ . The rate at which particles aggregate onto the surface to within a bond forming distance of an existing particle is smaller than  $\beta$  by a factor equal to the ratio of relevant areas and is given by  $\beta(2a\lambda)^2/4R^2$ . The average time of the latter aggregation process is, therefore,

$$t_\beta = R^2 / \beta(a\lambda)^2. \quad (25)$$

### C. Rearrangement

To calculate the average time of particle rearrangement, we employ a mean first passage time analysis similar to that employed for calculating particle dissociation rates described above. We again consider a surface where particles are arranged in a triangular lattice, as shown in Fig. 1. A particle is assumed to arrive at a random location on a representative lattice unit, triangle ABC, and diffuse on the surface towards the centroid of triangle ABC or to that of a nearby triangle. To describe this surface diffusion, we use polar coordinates with the centroid of triangle ABC as the origin. For simplicity, we assume the potential energy landscape to be radially symmetric, and write  $\Phi = \Phi(r)$ , where  $\Phi$  is the potential energy made dimensionless by the thermal energy  $kT$  is a function only of  $r$ , the radial distance from origin. The representative lattice unit and the energy landscape are shown schematically in Fig. 3.  $\Phi$  reaches a minimum at  $r = r_1 \geq 0$ , which marks the crystalline zone around the centroid. We let  $\Phi$  increase to a maximum at  $r = r_2$ , the edge of the potential well. The particle arrives onto the cluster surface into this potential well at  $r = r_o$  ( $r_1 \leq r_o \leq r_2$ ). Subsequently, the particle either diffuses to the minimum at  $r = r_1$ , or diffuses out of the well at  $r = r_2$  into one of the similar minima of adjacent wells. The diffusion in all wells being identical, we can assume that the particle is reflected back at the  $r = r_2$  bound-

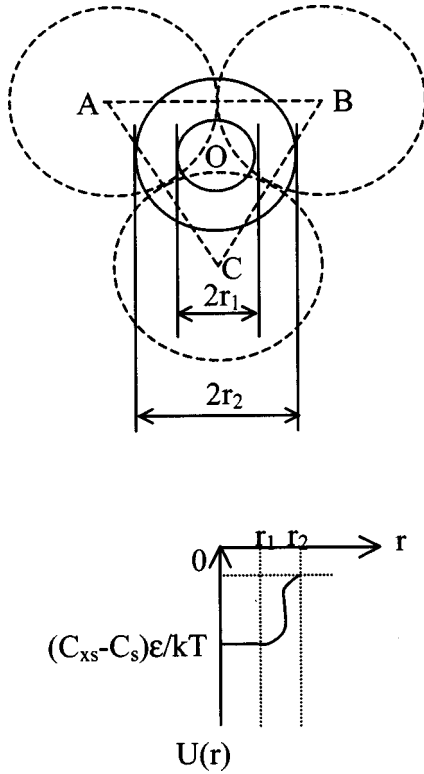


FIG. 3. An expanded view of a typical lattice unit showing the crystalline zone around the centroid (radius  $r_1$ ) and the edge of the amorphous zone (radius  $r_2$ ), and the corresponding potential energy landscape (bottom).

ary. Here, we calculate the time required for the particle to first reach the minimum at  $r_1$ .

Let  $w(r, t|r_o, 0)$  be the probability that the particle diffuses to a radial distance  $r$  at a time  $t$ , beginning from  $r_o$  at time  $t = 0$ . Our aim is to determine the evolution of this probability with respect to the initial position  $r_o$  for the fixed final position  $r = r_1$ . This evolution is governed by the backward Smoluchowski equation [19,21,30]:

$$\frac{\partial w(r, t|r_o, 0)}{\partial t} = D \left[ \frac{1}{r_o} \frac{\partial}{\partial r_o} \left( r_o \frac{\partial w(r, t|r_o, 0)}{\partial r_o} \right) - \left( \frac{\partial \Phi}{\partial r_o} \right) \left( \frac{\partial w(r, t|r_o, 0)}{\partial r_o} \right) \right]. \quad (26)$$

Solving this equation assuming an absorbing boundary at  $r = r_1$  and a reflecting boundary at  $r = r_2$  yields the average rearrangement time  $T(r_o)$  as [21,30]

$$T(r_o) = \frac{1}{D} \int_{r_1}^{r_o} \frac{e^{\Phi(r)}}{r} \int_r^{r_2} e^{-\Phi(r')} r' dr' dr. \quad (27)$$

To simplify this expression, we make the approximation that  $\Phi = \Phi_o$  at  $r = r_1$  and rises sharply to  $\Phi = 0$  for  $r > r_1$ . Then,  $\exp(-\Phi) \sim 1$  in the inner integral in Eq. (27). This yields

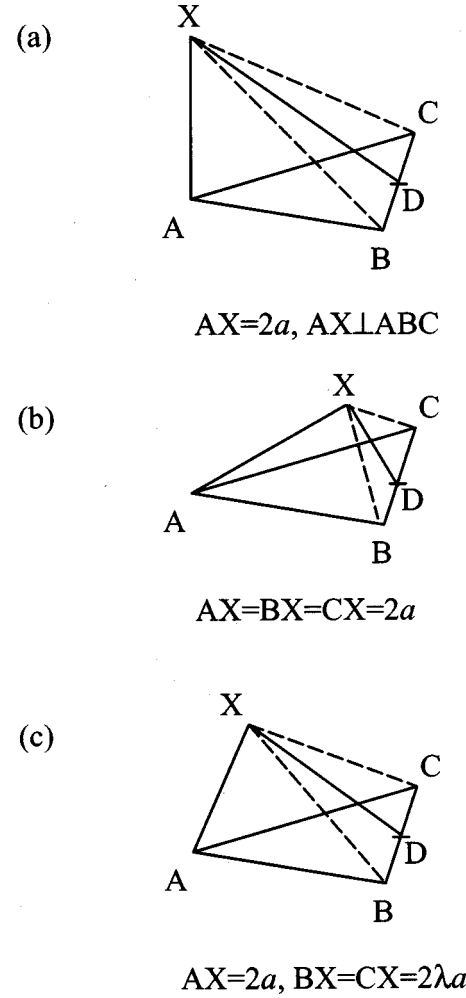


FIG. 4. Schematic representation of particle configurations to determine the sizes of the crystalline and amorphous zones on cluster surfaces. See text for description.

$$T(r_o) = \frac{1}{D} \int_{r_1}^{r_o} \frac{e^{\Phi(r)}}{r} \left( \frac{r_2^2 - r^2}{2} \right) dr. \quad (28)$$

Again, because of the sharply peaked nature of  $\Phi$ , most of the contribution to the above integral comes from the integrand near  $r = r_1$ . Therefore, nondimensionalizing the integrand and evaluating it at  $r/r_1 = 1$ , we get

$$T = (r_2^2 - r_1^2) e^{\Phi_o} / 2D. \quad (29)$$

To determine  $r_1$  and  $r_2$ , we consider a particle (center X) arriving directly onto one of the particles, say A, on the representative lattice unit ABC such that AX ( $= 2a$ ) is perpendicular to the plane ABC. The resulting arrangement is shown in Fig. 4(a). Since  $AB = 2a$ , we have  $BX = CX = (2\sqrt{2})a$ . Let D be the midpoint of BC. Then, from geometry,  $DX = \sqrt{7}a$ . Since the particle is driven equally by its attractions to the particles centered at B and C, we let it diffuse to a minimum energy location along the line DX. The

particle is closest to the plane ABC when ABCX forms a tetrahedron of side  $2a$  as shown in Fig. 4(b). Then,  $DX = \sqrt{3}a$ . This yields

$$r_2 = (\sqrt{7} - \sqrt{3})a. \quad (30)$$

Diffusing along DX, the particle first forms bonds with the particles B and C when  $BX = CX = 2\lambda a$ , as shown in Fig. 4(c). Then,  $DX = a\sqrt{(4\lambda^2 - 1)}$ , so that

$$r_1 = [\sqrt{(4\lambda^2 - 1)} - \sqrt{3}]a. \quad (31)$$

Substituting for  $r_1$  and  $r_2$  and noting that  $T = t_\gamma$ , we get

$$t_\gamma = \frac{a^2(4 - 2\lambda^2 - \sqrt{21} + \sqrt{12\lambda^2 - 3})\exp\{-(C_{xs} - C_s)\varepsilon/kT\}}{D_o\omega}, \quad (32)$$

where we have written  $\Phi_o = -(C_{xs} - C_s)\varepsilon/kT$  and  $D = D_o\omega$ , with  $\omega = 0.2$  again an approximate correction to  $D_o$  accounting for the near field hydrodynamic interactions of the particle diffusing on the cluster surface.

Finally, to calculate  $t_{\gamma x}$  the time for a particle in a crystalline location to diffuse to an amorphous location, the same backward Smoluchowski equation [Eq. (26)] is solved, except with a reflecting boundary condition at  $r = 0$  and an absorbing boundary condition at  $r = r_1$  [30]. Using similar simplifications as in deriving Eq. (32), we get

$$t_{\gamma x} = \frac{a^2(2\lambda^2 + 1 - \sqrt{12\lambda^2 - 3})\exp\{(C_{xs} - C_s)\varepsilon/kT\}}{D_o\omega}. \quad (33)$$

## V. MODEL PREDICTIONS OF GELATION AND CRYSTALLIZATION

To employ the above time scales for calculating the probabilities of gelation and crystallization, the parameters  $f$ ,  $C_{x\infty}$ , and  $\zeta$  must be determined. The distances  $r_1$  and  $r_2$  above allow the determination of the probability,  $f$ , that a particle arrives onto a cluster surface at a crystalline location. Assuming that particles arrive onto the surface at perfectly random locations (no steering),  $f$  is simply the ratio of the area of the crystalline zone to the total area of a lattice unit. Thus,  $f = (r_1/r_2)^2$ , or

$$f = \left( \frac{\sqrt{4\lambda^2 - 1} - \sqrt{3}}{\sqrt{7} - \sqrt{3}} \right)^2. \quad (34)$$

Note that  $f$  decreases as  $\lambda$  decreases, indicating that for shorter ranges of attraction particles are more likely to arrive into amorphous configurations. When  $\lambda = 1$ , all particles arrive in amorphous configurations as  $f = 0$ . On the other hand,  $f = 1$  for  $\lambda = \sqrt{2}$ , at which point all arriving configurations are energetically equivalent and are considered crystalline. Rearrangement is then driven by entropic effects. Here, we consider  $\lambda < 1.35$  to avoid the intervening stable fluid-fluid phase separation at higher  $\lambda$ . Under these circumstances, we assume that rearrangement is primarily enthalpic and neglect entropic effects.

To determine  $C_{x\infty}$ , we note that at the solubility boundary,  $\phi = \phi_s(\varepsilon/kT, \lambda)$ , only infinitely large clusters are stable, i.e., neither grow nor shrink. The stability of a cluster is determined by a balance between the rates of particle aggregation onto and dissociation from the cluster surface. The rate of particle aggregation onto a spherical cluster of radius  $R$  is given by  $\beta = R^2/a^2\lambda^2 t_\beta$ , where  $t_\beta$  is determined using Eq. (25). The number of particles on a cluster surface is [19]

$$N_s = 2\phi_{cp} \left( \frac{R}{a} \right)^3 \frac{[1 - (1 - a/R)^3]}{[1 - a/2R]}, \quad (35)$$

where  $\phi_{cp}$  is the packing fraction of particles on the cluster surface. Here, assuming the surface is densely packed, we let  $\phi_{cp} = 0.64$ . A fraction  $P_{\text{crystal}}/(P_{\text{crystal}} + P_{\text{gel}})$  of the particles on the surface may be assumed to reside in crystalline locations so that they dissociate with the time scale  $t_{\alpha x}$ . The remaining fraction dissociate with the time scale  $t_\alpha$ . Thus, the total dissociation rate is  $\alpha = [P_{\text{crystal}}/(P_{\text{crystal}} + P_{\text{gel}})](N_s/t_{\alpha x}) + [P_{\text{gel}}/(P_{\text{crystal}} + P_{\text{gel}})](N_s/t_\alpha)$ . At any  $\phi > \phi_s$ , the critical cluster size  $R^*$  is defined as that value of  $R$  at which  $\alpha = \beta$ , and is obtained by solving

$$\frac{P_{\text{crystal}}}{P_{\text{crystal}} + P_{\text{gel}}} \left( \frac{N_s}{t_{\alpha x}} \right) + \frac{P_{\text{gel}}}{P_{\text{crystal}} + P_{\text{gel}}} \left( \frac{N_s}{t_\alpha} \right) = \frac{(R^*)^2}{t_\beta(a\lambda)^2}. \quad (36)$$

For  $\phi = \phi_s$ ,  $R^* \rightarrow \infty$ . When  $R \gg a$ ,  $N_s = 6\phi_{cp}(R/a)^2$ ,  $t_{\alpha x} = Rde^{-\Phi}/D_o\omega$ , where  $\Phi = -C_{x\infty}\varepsilon/kT$ , and  $t_\alpha = Rde^{-\Phi}/D_o\omega$ , where  $\Phi = -(C_{x\infty} - 1.5)\varepsilon/kT$ . The aggregation rate for  $R \gg a$  and  $\phi = \phi_s \ll 1$  simplifies to  $\beta = 3RD_o\phi_s/a^3$ . Further,  $t_\gamma = a^2e^{-1.5\varepsilon/kT}[4 - 2\lambda^2 - \sqrt{21} + \sqrt{(12\lambda^2 - 3)}]/D_o\omega$  and  $t_{\gamma x} = a^2e^{1.5\varepsilon/kT}[2\lambda^2 + 1 - \sqrt{(12\lambda^2 - 3)}]/D_o\omega$ , where we have substituted  $C_{x\infty} - C_{s\infty} = 1.5$ . Since  $t_\gamma$  and  $t_{\gamma x}$  are independent of  $R$  for  $R \gg a$ , whereas  $t_\alpha$ ,  $t_{\alpha x}$ , and  $t_\beta$  increase with  $R$ , it follows that  $t_\gamma \ll t_\alpha, t_\beta$  and  $t_{\gamma x} \ll t_{\alpha x}, t_\beta$ . Equations (10)–(17) then simplify to yield  $P_r = P_{rx} = 1$  and  $P_{\text{crystal}}/P_{\text{gel}} = P_{ax}/P_a$ , where  $P_{ax} = t_{\gamma x}t_{\alpha x}/t_\beta(t_{\alpha x} + t_\beta)$  and  $P_a = t_\gamma t_\alpha/t_\beta(t_\alpha + t_\beta)$ . Equation (36) then becomes

$$\left( \frac{1}{1 + P_{ax}/P_a} \right) \left( \frac{\omega\phi_{cp}}{(\lambda - 1)\phi_s} \right) \left[ \frac{P_{ax}}{P_a} + e^{1.5\varepsilon/kT} \right] e^{-C_{x\infty}\varepsilon/kT} = 1, \quad (37)$$

where

$$\begin{aligned} \frac{P_{ax}}{P_a} = & \left( \frac{2\lambda^2 + 1 - \sqrt{12\lambda^2 - 3}}{4 - 2\lambda^2 - \sqrt{21} + \sqrt{12\lambda^2 - 3}} \right) \\ & \times \left( \frac{\omega + 6(\lambda - 1)\lambda^2\phi_s e^{(C_{x\infty} - 1.5)\varepsilon/kT}}{\omega + 6(\lambda - 1)\lambda^2\phi_s e^{C_{x\infty}\varepsilon/kT}} \right) \exp\left( \frac{4.5\varepsilon}{kT} \right). \end{aligned} \quad (38)$$

Solving these equations allows the determination of  $C_{x\infty}$ .

The parameter  $\zeta$ , which characterizes the variation of the number of nearest neighbors with the cluster radius  $R$ , is related to the curvature dependence of the solid-fluid surface tension. Thus, from knowledge of either the particle packing

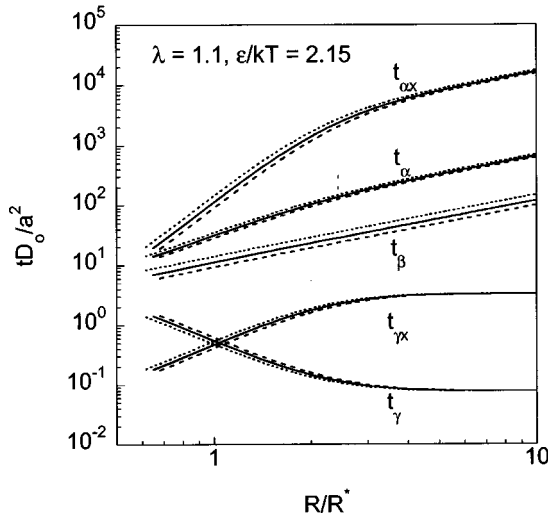


FIG. 5. Particle aggregation, dissociation, and rearrangement times calculated as described in the text at the interaction parameters shown for three volume fractions:  $\phi = 0.08$  (short dashed line), 0.10 (solid line), and 0.12 (long dashed line), plotted as a function of cluster size made dimensionless by the critical cluster size (see text) at each  $\phi$ .

profile or the curvature dependence of the surface tension,  $\zeta$  can be determined. Such information, however, is not available for square well systems. For hard-sphere suspensions,  $\zeta = 0.9$  results in good comparisons of model predictions of several measures of crystal nucleation kinetics with experimental estimates [18]. Here, we assume  $\zeta = 0.9$  to hold for square well systems as well and employ it for our calculations.

We note finally that the aggregation rate determined in Eq. (22) assumes the background monomer volume fraction to be fixed at  $\phi$ . In a suspension with  $\phi > \phi_s$ , however, multiple clusters can form and reduce the background monomer volume fraction below  $\phi$ . Indeed, detailed solutions of population balance equations to determine the time evolution of cluster size distributions during crystallization show that  $\phi$  quickly reduces to a steady value  $\phi_{\text{plat}}$ , at which much of crystal nucleation occurs [18]. Further, since the number densities of bigger clusters are small, an excellent estimate of  $\phi_{\text{plat}}$  is obtained by assuming that the suspension at this steady state consists of monomers and dimers alone and that equilibrium is established between the two species [18]. Following this description, we determine  $\phi_{\text{plat}}$  by solving

$$\phi_{\text{plat}} = \frac{\phi}{1 + \frac{2\beta(a, \phi_{\text{plat}})}{\alpha(R_{\text{min}})} \left(1 - \frac{\phi}{\phi_{cp}}\right)}, \quad (39)$$

where  $\alpha(R_{\text{min}}) = N_s/t_\alpha$  evaluated at  $R = R_{\text{min}}$  since at this size the distinction between crystalline and amorphous configurations ceases. The time scale for particle aggregation and all the quantities that follow are then determined by  $\phi_{\text{plat}}$  rather than  $\phi$ .

We present model calculations beginning in Fig. 5 with the time scales of the aggregation, dissociation, and rear-

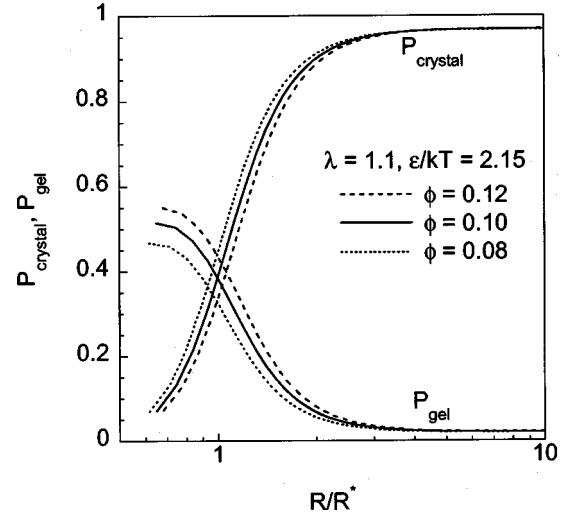


FIG. 6. Probabilities of crystalline and amorphous cluster formation at the conditions shown, plotted as a function of cluster size made dimensionless by the critical cluster size.

range processes. We present these time scales for the square well parameters  $\lambda = 1.1$  and  $\epsilon/kT = 2.15$  for three different particle volume fractions,  $\phi = 0.08, 0.10,$  and  $0.12$ . (For  $\lambda = 1.1$ ,  $\phi_b = 1.482$ , and  $f(\lambda) = -1.558$ , the parameter values necessary in Eq. (2) [23].) Under these conditions, we find  $\phi_s = 2.53 \times 10^{-3}$  and  $C_{x\infty} = 3.02$ . (We note that this is a small solubility but in line with those seen in protein crystallization experiments.) For the three volume fractions, we find that enough monomers are associated with clusters that the monomer volume fraction has been reduced to  $\phi_{\text{plat}} = 0.052, 0.062,$  and  $0.071$ , respectively. The time scales calculated as described in Sec. IV above are presented in Fig. 5 as functions of the cluster size  $R$  normalized with the critical cluster size  $R^*$  for each case. For the three volume fractions considered, we find  $R^*/a = 2.671, 2.510,$  and  $2.375$ , respectively. We note that for each  $\phi$ , the time scales follow the order  $t_{\alpha x}, t_\alpha, t_\beta, t_{\gamma x}, t_\gamma$  in decreasing order of their magnitudes. At a fixed  $\phi$ , the time scales increase with increasing  $R$ , except for  $t_\gamma$ , which decreases with increasing  $R$ . Similarly, at a fixed  $R/R^*$ , the time scales decrease upon increasing  $\phi$ , except for  $t_\gamma$  that follows the opposite trend.

These time scales determine the probabilities of crystallization and gelation which we present in Fig. 6. The probabilities are calculated using Eqs. (16) and (17) for the same conditions as in Fig. 5. For all values of  $\phi$  considered,  $P_{\text{crystal}} < P_{\text{gel}}$  for small  $R$ . As  $R$  increases,  $P_{\text{crystal}}$  increases whereas  $P_{\text{gel}}$  decreases so that  $P_{\text{crystal}} > P_{\text{gel}}$  for some sufficiently large  $R$ .

Of interest is the point of this crossover, i.e., the value of  $R$  at which  $P_{\text{crystal}} = P_{\text{gel}}$ , relative to the critical cluster size  $R^*$ . The critical cluster size determines the stability of clusters, clusters bigger than  $R^*$  grow, whereas clusters smaller than  $R^*$  shrink. When the crossover occurs at a value of  $R < R^*$ , stable clusters ( $> R^*$ ) tend to be crystalline as for the case where  $\phi = 0.08$  in Fig. 6. When the crossover occurs for  $R > R^*$ , stable clusters tend to be amorphous. This occurs for  $\phi = 0.12$  shown in Fig. 6. We note that for this latter case,

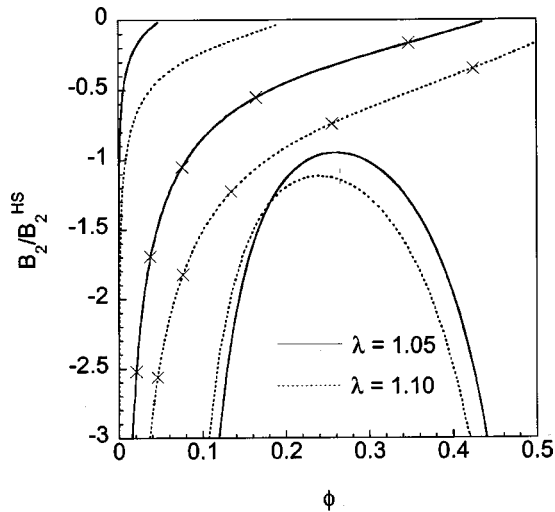


FIG. 7. Phase diagram for  $\lambda = 1.05$  (solid lines) and 1.1 (dashed lines) with the solubility boundary, the gel-crystal boundary, and the spinodal in that order upon going from left to right in the graph.

$P_{\text{crystal}} > P_{\text{gel}}$  for sufficiently large  $R$ . Thus, stable clusters that are amorphous when small can become crystalline, when sufficiently large. However, multiple clusters grow in solution simultaneously and if the crossover point occurs at sufficiently large  $R$ , these clusters can touch to form a gel before they can become crystalline. Identifying the precise volume fraction at which such a gel forms is difficult as it requires knowledge of the packing profiles of the amorphous clusters and the time evolution of the cluster size distribution. Here, we assume that if stable clusters are amorphous when small, they remain amorphous when large. Thus, the point where the crossover coincides with  $R^*$  marks the transition between where stable crystalline and amorphous clusters form. In Fig. 6, this occurs for  $\phi = 0.10$  and sets the gelation volume fraction  $\phi_g$  for  $\lambda = 1.1$  and  $\varepsilon/kT = 2.15$ .

Following this procedure, we calculate the gel-crystal boundary for a given range of attraction  $\lambda$ , as that value of  $\phi$ , called  $\phi_g$ , at each  $\varepsilon/kT$  at which

$$P_{\text{gel}}(R^*) = P_{\text{crystal}}(R^*), \quad (40)$$

where  $R^*$  is a function of  $\varepsilon/kT$  and  $\phi$ . In Fig. 7, we present the gel-crystal boundary for  $\lambda = 1.05$  and 1.1. (For  $\lambda = 1.05$ ,  $\phi_b = 1.370$ , and  $f(\lambda) = -1.118$  [23].) Also included in Fig. 7 are the solubility boundaries and the spinodals for  $\lambda = 1.05$  and 1.1 calculated as described in Sec. II. The phase boundaries are presented in  $B_2 - \phi$  space by converting  $\varepsilon/kT$  to  $B_2$  via Eq. (5). For both the values of  $\lambda$ , the gel-crystal boundary is located between the corresponding solubility boundary and the spinodal, the latter being metastable ( $\lambda < 1.35$ ). Thus, at a fixed value of  $B_2/B_2^{HS}$ , increasing  $\phi$  above  $\phi_s$  first produces crystals until the gel-crystal boundary is reached. Crossing the gel-crystal boundary, i.e., increasing  $\phi$  above  $\phi_g$ , results in the formation of stable amorphous clusters. If these clusters grow to span space, they lead to the formation of macroscopic gels. In this sense, the gel-crystal boundary is a lower limit on the volume fraction for gelation. Similarly, increasing the strength of particle attractions, i.e., lowering

$B_2/B_2^{HS}$ , at a fixed  $\phi$ , first results in crystals upon crossing the solubility boundary and then in amorphous aggregates upon crossing the gel-crystal line. Whether proceeding further into the spinodal results in gels or fluid-fluid phase separation remains to be understood. Further, the gel-crystal boundary shifts to lower volume fractions as  $\lambda$  decreases from 1.1 to 1.05. Thus, at a fixed average attraction or  $B_2/B_2^{HS}$ , decreasing the range of attraction leads to an increased tendency to form gels.

Figure 7 summarizes model predictions of the effects of changing the particle concentration and the strength and the range of particle attractions on the resulting gelation and crystallization transitions. At this point, several comments about the predictions are in place. We emphasize that the gel-crystal boundary is different from the other phase boundaries in Fig. 7 in that traversing across the gel-crystal boundary does not produce a reversible crystal-gel transition. What the gel-crystal boundary tells is whether the transition that results upon quenching a suspension rapidly to a particular region in the phase diagram is crystallization or gelation. More precisely, it tells whether the stable clusters that form are crystalline or amorphous.

We note next that at a fixed  $B_2/B_2^{HS}$ , although the volume fraction at the gel-crystal boundary, i.e.,  $\phi_g$ , decreases as the range of attractions is decreased,  $\phi_g$  always remains higher than the equilibrium solubility  $\phi_s$  at that  $B_2/B_2^{HS}$ . In the present description,  $R^*$  diverges at the solubility boundary so that no stable clusters can nucleate for  $\phi < \phi_s$ . Thus,  $\phi_g$ , which determines where stable amorphous clusters nucleate, is bounded below by  $\phi_s$ . We note further that  $\phi_s$  is determined in this description using equilibrium thermodynamics as the volume fraction above which the lowest free energy state of the system is a solid, in the interior of which particles have  $C$  nearest neighbors [Eq. (4)]. In calculating  $R^*$ , however, only a description of the surface of such a solid is considered [Eq. (36)]. Therefore, implicit in letting  $R^*$  diverge at  $\phi_s$  [Eqs. (37) and (38)] is the assumption that the interiors of nucleating clusters have the same properties as the stable solid dictated by equilibrium thermodynamics. The description of the solid chosen is usually based on observations of the resulting crystal structures, e.g., the standard choice of  $C = 12$  is motivated by the fcc or hcp structure.

Often, however, such a description cannot be identified uniquely. For instance, in suspensions where the particles have a significant size polydispersity, the crystalline free energy minimum is suppressed for the solid [31]. This makes identifying  $\phi_s$  ambiguous. Under these circumstances,  $\phi_s$  identified by assuming a particular solid structure does not rule out the occurrence of stable clusters corresponding to other structures for  $\phi < \phi_s$ . In particular, amorphous structures leading to gels may occur for  $\phi < \phi_s$ , suggesting that under some conditions  $\phi_g < \phi_s$ . Indeed, in recent experiments on colloid-polymer mixtures, gels have been observed to preempt crystallization for small polymer-to-colloid size ratios or small ranges of attraction [9,10]. Whether this implies that  $\phi_g < \phi_s$  or whether gels are observed upon crossing the gel-crystal boundary for  $\phi_g > \phi_s$  due to slow crystal nucleation kinetics for  $\phi < \phi_g$  remains to be verified. That

crystal nucleation can be slow for  $\phi < \phi_g$  is seen in experiments on globular protein suspensions where crystals are not observed at low strengths of attraction, where the supersaturations are low, until the gel boundary, but are observed at higher strengths of attraction, where much higher supersaturations are attained, before gel formation [12]. At the same time, simulations of hard-sphere suspensions have suggested that size polydispersity can lower crystal nucleation rates by several orders of magnitude [32].

We remark next that the local description leading to the arrest of particles on cluster surfaces employed in the present model is somewhat similar to the description of cages employed in recent mode-coupling approaches [16]. In the latter approaches, particularly applicable to dense suspensions, particles are assumed to be trapped in cages formed by other similar particles. The diffusion of particles therefore requires the breakup of these cages. In analogy, we assume that particle motion on cluster surfaces is possible only when no additional particles peg it on the surface. Mode-coupling theory assumes, however, that structural relaxation occurs via cooperative motion of the particles, whereas such relaxation mechanisms are neglected in the present approach.

Finally, we mention two approximations that introduce uncertainties in model predictions. First, the rearrangement time of individual particles is calculated assuming diffusion on a perfectly crystalline surface. A cluster surface, however, has both crystalline and amorphous regions. Rearrangement on amorphous regions must necessarily be cooperative and is therefore expected to be slower than on crystalline regions. As a result, the model overestimates the tendency for crystallization. Second, any steering of arriving particles into energetically favorable configurations is assumed to be absent. Steering would enhance the tendency to form crystals beyond what is predicted in Fig. 7 as the range of attractions increases. Despite these limitations, model predictions are in qualitative agreement with experiments [8–11]. To test the predictions quantitatively, we turn next to comparisons with experiments.

The competition between gelation and crystallization has been best studied with colloid-polymer mixtures [8–11]. However, comparisons with these experiments require significantly different descriptions of the fluid and solid phases, in particular, incorporating polymer partitioning in the two phases. Explicit two-component descriptions have been developed that capture the equilibrium phase behavior of colloid-polymer mixtures [9,10,33], but the kinetics of the phase transitions remains poorly understood. In the present description, colloidal suspensions are treated as one-component systems with the particles interacting via an effective interaction potential. Such descriptions have proven successful in describing the phase behavior of inherently attractive systems (as opposed to colloid-polymer mixtures where the attraction between the particles is induced by adding polymer) such as globular proteins [27,28]. Here, we compare model predictions with recent experiments on globular proteins [12].

In Fig. 8, we present the experimental phase behavior recently reported for lysozyme in phosphate buffer solution [12]. The solubility boundary is shown by triangles and the

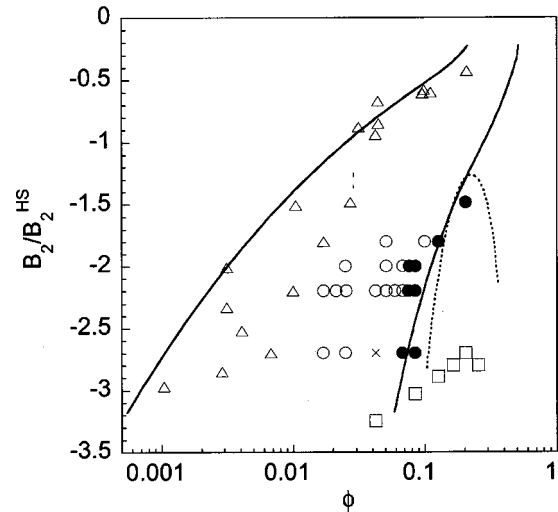


FIG. 8. Model predictions of the phase diagram for  $\lambda=1.15$  compared with the experiments reported in Ref. [12]. The symbols are described in the text.

fluid-fluid phase boundary by squares. That the fluid-fluid phase boundary is metastable with respect to the solubility boundary indicates that the proteins experience short-range attractions. The dynamics of structural relaxation of suspensions spanning a wide range of conditions between these boundaries was studied. Where density fluctuations relaxed within experimental time scales, the suspensions were considered fluidlike. Fluidlike conditions are shown in Fig. 8 as open circles. Where density fluctuations failed to relax completely, the suspensions were considered nonergodic, indicating the onset of gelation. Such conditions are shown as solid circles in Fig. 8. Finally, visual inspection allowed the detection of crystals. Suspensions where crystals were seen are shown in Fig. 8 as crosses.

To make comparisons with this data, we present in Fig. 8, calculations of the solubility boundary, the spinodal, and the gel-crystal boundary as outlined above for  $\lambda=1.15$  (for which  $\phi_b=1.580$  and  $f(\lambda)=-1.957$  [23]). Quite remarkably, both the solubility boundary and the gel-crystal boundary are in excellent agreement with experiments. Here, we assume that at lower strengths of attraction where crystals are not seen, the gel-crystal boundary is given by the transition between the open and solid circles, as crystals are expected to nucleate in supersaturated suspensions upon waiting sufficiently long.  $\lambda=1.15$  is chosen to give the best fit. The poor agreement between the predicted spinodal and the experimental fluid-fluid phase boundary has been attributed to the anisotropic nature of protein interactions [29,34].

The remarkable agreement between model predictions and experiments gives us confidence that the model captures the underlying physics of the competition between gelation and crystallization in attractive colloidal suspensions. However, more rigorous tests of the model are necessary for verifying this description, particularly, since square well interactions are known to be oversimplified representations of protein interactions. Not only the location of the spinodal, but the kinetics of crystallization in proteins is also not captured via square well attractions [19,35]. More detailed de-

descriptions of the aggregation and dissociation processes for particles interacting with anisotropic attractions have been developed and have been shown to capture the kinetics of protein crystallization better [20]. Descriptions of the rearrangement processes for such interactions must be developed and the present model adapted accordingly.

A limitation of the present comparison is its inability to capture the competition between crystallization and glass formation observed in hard-sphere suspensions: Hard-sphere suspensions crystallize above  $\phi \sim 0.495$  and form glasses above  $\phi \sim 0.58$  [13]. In the present description, hard-sphere interactions occur in the limit  $\varepsilon/kT=0$ . Extrapolation of the above calculations to this limit does not result in the observed behavior for hard-sphere suspensions for two reasons. First, the equation of state for square well particles employed here [Eq. (2)] is an empirical fit to simulation data and fails to predict the hard-sphere solubility boundary in the limit  $\varepsilon/kT=0$  [23]. Second, particle dissociation kinetics in the hard-sphere limit are governed by the potential of mean force [17,18], which is neglected in the present description since it is small compared to inherent particle attractions, especially in the low volume fraction limit where the competition between gelation and crystallization in globular protein suspensions is observed.

Another limitation of the above comparison is that the data is insufficient to test the effect of the range of particle attractions on the location of the gel-crystal boundary. Such a test requires experiments where the range of the attractions is carefully tuned as possible in the case of colloid-polymer mixtures. However, the need to account for polymer partitioning in order to compare with these experiments necessitates a significant modification to the present description of the thermodynamics of solid and fluid phases and is beyond the scope of the present paper.

## VI. CONCLUSIONS

We have presented a model for predicting the occurrence of gelation and crystallization in attractive square well sys-

tems as a competition between particle aggregation, dissociation, and rearrangement processes. The model is based on a kinetic model of crystal nucleation that accounts for the average times of aggregation and dissociation processes. A mean first passage time analysis has been developed to calculate the time require for particle rearrangement. Based on the relative magnitudes of these time scales, the probability that a particle aggregating onto a cluster surface rearranges to a crystalline location or remains trapped in an amorphous configuration is determined. Depending on which of these events is the most probable, the occurrence of crystals or amorphous clusters, which act as precursors to gels, is predicted.

From these calculations, we locate the crystal-gel boundary by identifying at each  $\varepsilon/kT$ , the minimum value of  $\phi$ , called  $\phi_g$ , at which the probability of forming amorphous clusters is higher than that of forming crystalline clusters.  $\phi_g$  thus provides a lower bound on the volume fraction for gelation. At any  $\varepsilon/kT$ , crystals result for  $\phi_s < \phi < \phi_g$ , whereas gels result for  $\phi > \phi_g$ . The predictions are compared with recent experiments on globular protein suspensions. The model predictions for the range of attraction,  $\lambda = 1.15$ , are in excellent agreement with the gel-crystal line observed experimentally. This gives us confidence that the model captures much of the underlying physics of the competition between gelation and crystallization. Further studies are necessary to test the ability of the model to predict the effect of the range of particle interactions on the resulting gelation and crystallization transitions.

## ACKNOWLEDGMENTS

The authors acknowledge support from the U.S. DOE via the University of Illinois at Urbana-Champaign, Frederick Seitz Materials Research Laboratory, Grant No. DEFG0296ER45439. N.M.D. thanks Shivashankar Chetan for insightful discussions.

- 
- [1] C. J. Brinker and G. W. Scherer, *Sol-Gel Science: The Physics and Chemistry of Sol-Gel Processing* (Academic, Boston, 1990).
  - [2] W. C. K. Poon, P. N. Pusey, and H. N. W. Lekkerkerker, *Phys. World* April, 27 (1996).
  - [3] V. Trappe and D. A. Weitz, *Phys. Rev. Lett.* **85**, 449 (2000).
  - [4] M. Muschol and F. Rosenberger, *J. Chem. Phys.* **107**, 1953 (1997).
  - [5] D. F. Rosenbaum and C. F. Zukoski, *J. Cryst. Growth* **169**, 752 (1996).
  - [6] A. McPherson, *Preparation and Analysis of Protein Crystals* (Kreiger, Melbourne, FL, 1982).
  - [7] J. Aizenberg, P. V. Braun, and P. Wiltzius, *Phys. Rev. Lett.* **84**, 2997 (2000).
  - [8] S. M. Ilett, A. Orrock, W. C. K. Poon, and P. N. Pusey, *Phys. Rev. E* **51**, 1344 (1995).
  - [9] S. Ramakrishnan, M. Fuchs, K. S. Schweizer, and C. F. Zukoski, *J. Chem. Phys.* **116**, 2201 (2002).
  - [10] S. A. Shah, Y.-L. Chen, K. S. Schweizer, and C. F. Zukoski, *J. Chem. Phys.* **118**, 3350 (2003).
  - [11] P. N. Segre, V. Prasad, A. B. Schofield, and D. A. Weitz, *Phys. Rev. Lett.* **86**, 6042 (2001).
  - [12] A. M. Kulkarni, N. M. Dixit, and C. F. Zukoski, *Faraday Discuss.* **123**, 37 (2003).
  - [13] W. B. Russel, D. A. Saville, and W. R. Schowalter, *Colloidal Dispersions* (Cambridge University Press, Cambridge, 1989).
  - [14] M. C. Grant and W. B. Russel, *Phys. Rev. E* **47**, 2606 (1993).
  - [15] M. G. Noro, N. Kern, and D. Frenkel, *Europhys. Lett.* **48**, 332 (1999).
  - [16] J. Bergenholtz, M. Fuchs, and T. Voigtmann, *J. Phys.: Condens. Matter* **12**, 6575 (2000).
  - [17] N. M. Dixit and C. F. Zukoski, *Phys. Rev. E* **64**, 041604 (2001).

- (2001).
- [18] N. M. Dixit and C. F. Zukoski, Phys. Rev. E **66**, 051602 (2002).
- [19] N. M. Dixit and C. F. Zukoski, J. Colloid Interface Sci. **228**, 359 (2000).
- [20] N. M. Dixit and C. F. Zukoski, J. Chem. Phys. **117**, 8540 (2002).
- [21] G. Narasimhan and E. Ruckenstein, J. Colloid Interface Sci. **128**, 549 (1989).
- [22] Y. C. Chiew and E. D. Glandt, J. Phys. A **16**, 2599 (1983).
- [23] S. Ramakrishnan and C. F. Zukoski, J. Chem. Phys. **113**, 1237 (2000).
- [24] D. M. Heyes and P. J. Aston, J. Chem. Phys. **97**, 5738 (1992).
- [25] N. Asherie, A. Lomakin, and G. B. Benedek, Phys. Rev. Lett. **77**, 4832 (1996).
- [26] A. Lomakin, N. Asherie, and G. B. Benedek, J. Chem. Phys. **104**, 1646 (1996).
- [27] D. F. Rosenbaum and C. F. Zukoski, J. Cryst. Growth **169**, 752 (1996).
- [28] D. F. Rosenbaum, P. C. Zamora, and C. F. Zukoski, Phys. Rev. Lett. **76**, 150 (1996).
- [29] A. M. Kulkarni, Ph.D. thesis, University of Illinois, 2001.
- [30] C. W. Gardiner, *Handbook of Stochastic Methods* (Springer-Verlag, New York, 1983).
- [31] P. Sollich, J. Phys.: Condens. Matter **14**, R79 (2002).
- [32] S. Auer and D. Frenkel, Nature (London) **409**, 1020 (2001).
- [33] H. N. W. Lekkerkerker, W. C. K. Poon, P. N. Pusey, A. Stroobants, and P. B. Warren, Europhys. Lett. **20**, 559 (1992).
- [34] R. P. Sear, J. Chem. Phys. **111**, 4800 (1999).
- [35] N. M. Dixit, A. M. Kulkarni, and C. F. Zukoski, Colloids Surf., A **190**, 47 (2001).